Batteries & Supercaps

Concept
doi.org/10.1002/batt.202200359

Chemistry Europe
European Chemical Societies Publishing

www.batteries-supercaps.org

Progress of Atomic Layer Deposition and Molecular Layer Deposition in the Development of All-Solid-State Lithium Batteries

Yu Su,[a] Jialiang Hao,[a] Xiangsi Liu,[a] and Yong Yang*[a, b]

As one of the most promising candidates for next-generation high-energy storage systems, all-solid-state lithium batteries (ASSLBs) including the bulk-type and thin-film-type configurations have attracted great attention currently. The rational construction of the electrodes and electrolytes, as well as well-controlled interface modification, are indispensable for realizing the practical application of ASSLBs. In recent decades, atomic layer deposition (ALD) and molecular layer deposition techniques (MLD) have been widely applied as powerful tools to achieve the accurate control of atomic/molecular thickness and composition adjustment of the thin protective layers or electrodes. Owing to the unique features, ALD/MLD techniques show great potential in manipulation of interfacial properties and constructing novel electrode structures in the research of ASSLBs. In this review, we highlight the recent progress in the developments and applications of ALD/MLD techniques in ASSLBs, including the interface modification for both cathodes and lithium metal anodes in bulk-type ASSLBs, and the preparation of electrodes and solid electrolytes in thin-film type batteries. In addition, an overview of the existing challenges and the application prospects of ALD/MLD in ASSLBs are also presented.

1. Introduction

As our society shifts from fossil energy to renewable energy, the demand for sustainable energy has greatly promoted the research of low-cost, environmentally friendly, and high-efficiency energy conversion and storage devices.[1] Owing to the outstanding energy density and long cycle life, lithium-ion batteries (LIBs) have dominated the electrochemical energy storage field for decades. However, based on liquid electrolytes (LEs), the developments of conventional LIBs have reached a bottleneck in terms of increasing the energy density of batteries. Furthermore, the rapid developments of large-scale energy storage devices, such as electric vehicles and smart grids, have put forward urgent demands for enhancing the safety of batteries.[2,3]

Although LEs possess the advantages of high ionic conductivity and flexible electrode wettability, they also suffer from many shortcomings such as the low transference number, inferior thermal stability, and flammability.[4] In this respect, the utilization of non-flammable solid-state electrolytes (SSEs) is expected to break the above limitations of LEs, allowing conceptual innovations in battery configuration and realizing functional structure design.[2] Besides, some SSEs (such as garnet-type SSEs) could show a wider electrochemical window than that of their liquid counterparts, which enables the battery to obtain a high energy density.[5] In addition, the stable and rigid SSEs are expected to suppress the continuous reactions between Li and electrolyte, and the growth of notorious lithium dendrites, thereby realizing a rechargeable Li metal battery with long cycles.[6]

According to the solid electrolyte thickness and the cell configuration, ASSLBs can be divided into two main categories including bulk-type and thin-film-type ASSLBs. For the bulk-type ASSLBs, although the ionic conductivity of some bulk SSEs (especially argyrodite-type sulfide SSEs) has reached or is even higher than LEs, the energy density, rate capability and cyclability of ASSLBs still cannot meet the requirements of practical applications.[7–9] Currently, many researchers suggest that the primary cause for the inferior ASSLBs performance is the large interfacial resistance between the electrode and SSEs, which originates from the mechanical force development and the chemical composition changes.[10–13] Therefore, much effort has been devoted to improving the electrochemical performance of bulk-type ASSLBs through the cell structural design and the interfacial modification between the electrolyte and electrode.[14]

Different from the bulk-type ASSLBs, the thin-film-type ASSLBs are mainly used in low-power microelectronics and energy harvesting technologies. Of note, the unique main advantage of thin-film type ASSLBs is micro battery assemblies, especially three-dimensional (3D) micro-batteries, which greatly shorten the transport distance of carrier ions, endowing the

[a] Y. Su, J. Hao, X. Liu, Prof. Y. Yang
State Key Laboratory for Physical Chemistry of Solid Surface Department of Chemistry
College of Chemistry and Chemical Engineering
Xiamen University
361005 Xiamen, Fujian, China
E-mail: yyang@xmu.edu.cn
[b] Prof. Y. Yang
College of Energy
Xiamen University
361005 Xiamen, Fujian, China
E-mail: yyang@xmu.edu.cn

This publication is part of a joint Special Collection on Solid State Batteries, featuring contributions published in Advanced Energy Materials, Energy Technology, Batteries & Supercaps, ChemSusChem, and Advanced Energy and Sustainability Research.

fast ion transport kinetics and excellent rate performance.[15] Furthermore, the performance of thin-film type ASSLBs can be further improved by carefully adjusting the physical and chemical properties of electrode and electrolyte films.[16] Thus, the further development of appropriate thin-film growth techniques is the key point for controllable interface modification and battery component construction.[17]

To date, various deposition strategies have been used to improve the (electro) chemical stability of electrode/SSE materials, including solution method, sol-gel method,[18] physical vapor deposition (PVD),[19] pulsed laser deposition (PLD),[20] chemical vapor deposition (CVD),[21] and atomic/molecule layer deposition (ALD/MLD).[22] As shown in Table 1, with a comparison of all kinds of film deposition methods, ALD and MLD techniques show unique advantages in many aspects. In particular, different from solution-based deposition (solution method and the sol–gel method), ALD/MLD techniques offer precisely thickness-controlled layers with excellent uniformity and conformality at the nanometer or even angstrom level. Moreover, although both CVD and ALD techniques are capable of producing conformal layers on complex three-dimensional substrates, the film deposition could be implemented at lower temperatures by ALD/MLD technique compared to CVD methods. In addition, thanks to the rapid developments of industrial equipment (such as fluid-bed atomic layer deposition), mass production is no longer a major concern which limits the practical application of ALD and MLD techniques.[23]

Although there are several good reviews on ALD/MLD techniques for solid-state batteries have been published,[24–26] they are more focused on the application of ALD technique in the field of bulk-ASSLBs. While the purpose of this review is not only to critically review representative examples and state-of-art of the applications of ALD/MLD techniques on the surface modification of the electrode/electrolyte materials in bulk-type but also in thin-film-type ASSLBs. Particularly, we also highlight the newest application of the ALD/MLD technique in the preparation of electrode & electrolytes materials for ASSLBs. In detail, we first give a brief introduction to ALD/MLD techniques and then summarize the interface modification of ALD/MLD for bulk-type ASSLBs. This section mainly focuses on the fabrication and function of electrodes' coating layer by ALD/MLD. Afterward, we overview the recent progress in the preparation of electrode and electrolyte materials in 2D and 3D thin-film-type micro-ASSLBs. In the last section, we present a personal perspective on the future development and application of ALD/MLD in ASSLBs.

2. The Introduction of ALD/MLD Techniques

Since Suntalo and co-workers put forward the atomic layer epitaxy technique in the 1970s, the ALD technique has made great progress in the field of microelectronics industry and nanotechnology. In 2001, ALD was listed as a candidate technology compatible with the microelectronics industry by the International Semiconductor Industry Association. The above achievements are inseparable from its unique self-limiting growth principle and a complete ALD/MLD deposition

Yu Su received her Bachelor's degree in Beijing Institute of Technology in 2019. She is now a Ph.D. candidate in School of Chemistry and Chemical Engineering, Xiamen University supervised by Prof. Yong Yang. Her research focuses on the application and development of ALD/MLD technique in sulfide-based solid-state batteries.

Jialiang Hao received his Bachelor's degree in chemistry from Ocean University of China in 2019. He is currently working towards a master's degree in Chemical Engineering under the supervision of Prof. Yong Yang at Xiamen University. His research focuses on the synthesis and modification of Ni-rich NMC cathode materials for Li-ion batteries.

Xiangsi Liu received his Bachelor's degree in Nanjing University of Aeronautics and Astronautics in 2017. He is now a Ph.D. candidate in School of Chemistry and Chemical Engineering, Xiamen University supervised by Prof. Yong Yang. His research focuses on understanding the reaction mechanism of LIBs and NIBs by solid-state NMR and developing high-performance energy storage materials.

Yong Yang is a distinguished professor in Chemistry in the State Key Lab for Physical Chemistry of Solid Surface at Xiamen University since 1997. He now also serves as Editor for J. Power Sources, Board Member of international Battery Materials Association (IBA) and International Meeting of Lithium Battery (IMLB). His main research interests are new electrode/electrolyte materials for Li/Na-ion batteries, in situ spectroscopic techniques, and interfacial reaction mechanism study in electrochemical energy storage and conversion system.

Table 1. A Comparison of the advantage of different film deposition techniques.

Method	Uniformity and smoothness	Conformality	Deposition at low temperature	Single atomic layer film	Controllable thickness	A fully dense deposition is common
Solution method	Low	×	√	×	×	×
Sol-gel method	Low	×	√	×	×	×
Chemical vapor deposition (CVD)	Varies	Varies	×	×	√	√
Physical vapor deposition (PVD)	Medium	for flat samples only	√	×	√	√
Pulsed laser deposition (PLD)	Medium	for flat samples only	√	×	√	√
Atomic/molecule layer deposition (ALD/MLD)	High	High	√	√	√	√

processes with different oxidizing or hydrolysis regents such as O_3, H_2O and EG in different reaction paths are depicted in Figure 1. Especially, there are four steps in each subcycle: 1) precursor A [such as trimethyl aluminum (TMA)] reacts with the surface functional groups of substrates; 2) the inert gas (N_2 or Ar) removes the unreacted precursor A; 3) precursor B [such as H_2O or ethylene glycol (EG)] reacts with the surface functional groups generated from step (1); 4) the inert gas removes the unreacted precursor B and by-products. By repeating the above four steps, the thickness of the deposited film increases. Thus, it can achieve layer-by-layer control of material growth at the angstrom or monolayer level.

Moreover, the self-limiting aspect of ALD/MLD can achieve extremely high uniformity of the synthesized film on high aspect ratio structures, since ALD/MLD belong to the surface chemical saturation adsorption process. In detail, part of surface areas will react before other areas due to different precursor gas fluxes, the precursors will be desorbed from the surface area completed by the reaction. Then, the precursor will continue to react with other unreacted surface areas and produce very conformal deposition on the substrate with any complex morphology. Due to there are no surface sites left in the film growth process, the film is continuous without pinholes.[27]

The types and quantities of materials prepared by ALD have achieved explosive development in recent years which covers a variety of inorganic materials including the elementary substance, oxide, nitride, sulfide, fluoride, selenide, telluride, carbide, etc. As a derivative of ALD technique, MLD technique greatly expands the range of film types, especially for the organic thin film. By pairing the metal precursor with the organic reactant source to add molecular fragments to the film, materials prepared by ALD/MLD can be extended from traditional inorganic materials to polymers and inorganic-organic

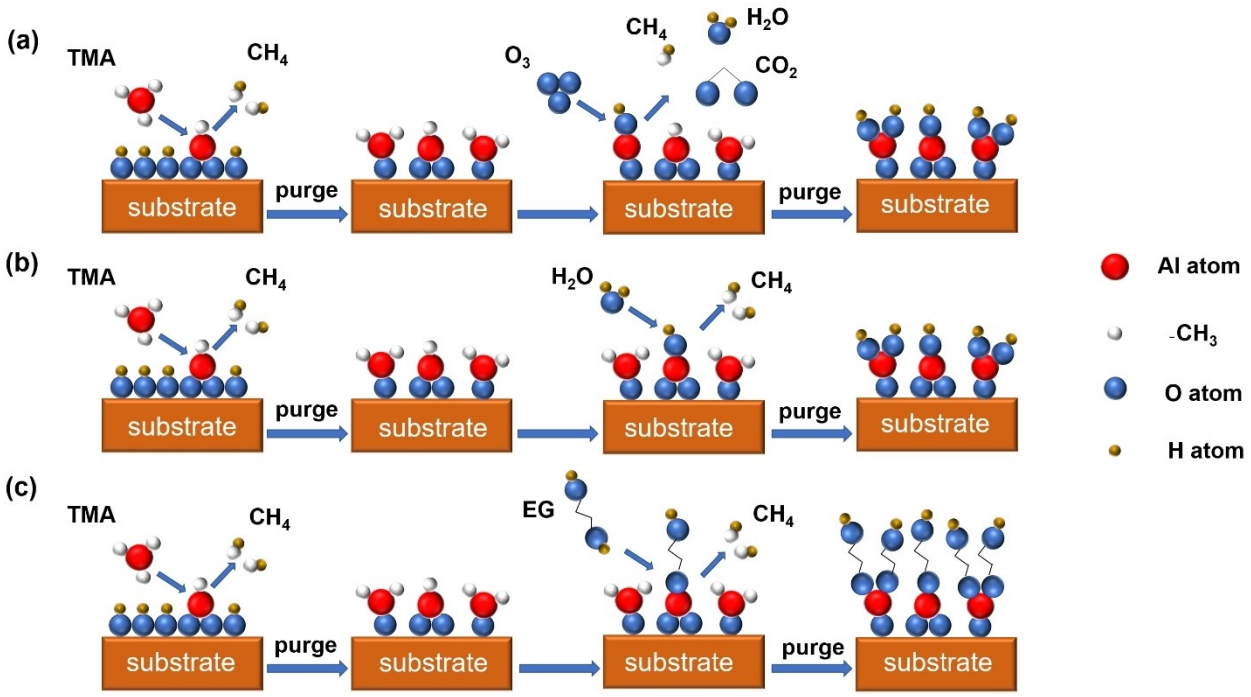

Figure 1. Schematic diagrams of ALD/MLD methods for production of thin films with precursors of trimethyl aluminum (TMA) and a) O_3, b) H_2O for Al_2O_3 and c) EG for Alucone.

hybrid materials. Furthermore, with the suitable precursors and deposition process, the mechanical, electrical, optical, and electrochemical properties of the film can be controlled at the atomic/molecular level. The above unique advantages make ALD/MLD techniques stand out from all other deposition approaches in the application of ASSLBs.[28]

On the other hand, the application of bulk ASSLBs is limited by the large electrode/electrolyte interfacial impedance, while the abundant thin-film materials deposited by ALD/MLD can be used for interfacial modification coatings. Besides, they could precisely control the thickness and composition of the coating material, i.e., the thickness can even be accurate to the sub-nanometer level. Therefore, ALD/MLD technique has been widely studied to modify the surface of electrodes to effectively improve electrochemical performance. In addition, ALD/MLD can also provide electrode and electrolyte synthesis for thin-film ASSLBs, and three-dimensional micro-batteries can be fabricated by conformal deposition on three-dimensional substrates. To sum up, the main application aspects of ALD/MLD in ASSLBs include: 1) the synthesis of nanostructured electrodes, 2) the fabrication of solid electrolytes, and 3) the modification of the electrode/electrolyte interface.

3. The Application of ALD/MLD Techniques in Bulk ASSLBs

Rapid progress has been achieved in the development of a series of solid electrolyte materials with high ionic conductivity in recent years, which includes inorganic (perovskite, NASICON-type, garnet, sulfide solid electrolyte, and halide solid electrolytes), organic (polymer-type), and organic-inorganic composite SSEs.[2,29] Among them, argyrodite-type sulfide SSEs exhibit the highest lithium ion conductivity, even beyond the level of LEs.[30] Moreover, the reasonable mechanical nature of sulfide-based SSEs makes them easier to press into shape and thus meet the basic requirement of scientific research. Unfortunately, based on sulfide-based SSEs, bulk-type ASSLBs still cannot deliver an acceptable electrochemical performance since the large interfacial impedances of cathode/SSEs and SSEs/lithium metal anode interfaces.[31,32] For example, Mo et al. showed that sulfide-based SSEs only show a narrow electrochemical window based on first-principles calculations, which is consistent with the experimental results that the decomposition of sulfide-based SSEs occurs at the beginning of charging and intensifies significantly with the increase of applied voltage.[33,34] Besides, recent studies revealed that the cathode active materials usually suffer from the large volume change, resulting in obvious voids between the active material and SSEs after charge/discharge cycles.[35,36] More recently, single-crystal materials show good compatibility with SSEs owing to their better mechanical stability than that of their polycrystalline counterpart, while the serious interface problems still need to be solved urgently.[11,37] For the anode side, especially for the lithium metal, the contact failure and interface side reactions would become more serious due to the deposition-dissolution reaction mechanism and the strong reactivity of lithium metal. Furthermore, the growth of lithium dendrites also cannot be ignored in ASSLBs configuration.

To sum up, on the cathode side, the capacity-decay mechanism of the chemo-mechanical coupling between the cathode and the electrolyte requires the optimal design of the interface to make it stable and flexible.[38] On the anode side, in addition to the interface impedance caused by poor physical contact and chemical reactions between the bulk solid electrolytes and lithium metal anode, the growth of lithium dendrites cannot be ignored for the destruction of the solid electrolyte.[39,40] Therefore, the introduction of a coating layer is deemed as a simple and effective way to alleviate the above-mentioned interfacial issues in ASSLBs. In general, the coating layers on both electrodes in ASSLBs are required to have the following characteristics: 1) high ionic conductivity to ensure fast Li^+ transport, 2) wide electrochemical window to match the high voltage cathode and low potential anode, and 3) sufficient mechanical strength and flexibility to accommodate the volumetric changes of electrodes during cycling. In this section, we have selected typical examples to show how ALD/MLD techniques are capable of constructing functional layers for high-performance ASSLBs.

4. Cathode Interface Modifications

4.1. Interfacial materials fabrication by ALD/MLD technique

ALD/MLD technique was used in the coating of cathode materials for liquid batteries in the early stage. By accurately adjusting the thickness of ALD coating layer, George et al. discovered for the first time that even a few angstroms thickness of Al_2O_3 film can achieve excellent electrochemical performance of $LiCoO_2$ and graphite electrodes.[41] Later, they extend this strategy to manipulate the interfacial properties in ASSLBs by ALD technique.[42]

The requirements for the interfacial coating materials for ASSLBs are thin film, highly conductive and chemically/electrochemically stable. Generally, ionic compounds with highly positively charged cations (such as Nb^{5+}, Ta^{5+}, and P^{5+}) have excellent oxidation stability and a low tendency to release oxygen at high potentials.[43] On the other hand, although metal oxides coatings effectively inhibit the side reactions between the oxide-type cathode and solid electrolytes, its low lithium-ion conductivity and even ion insulation will cause a large initial impedance in bulk ASSLBs. Therefore, lithium-containing thin films with positively charged cations are the ideal candidates in the bulk ASSLBs. In this respect, ALD can easily synthesize the desired multicomponent compounds by combining suitable precursors. Moreover, Mo's calculation shows that the introduction of an interface layer between the cathode and SSE can inhibit the parasitic reactions, such as $LiNbO_x$, $LiTiO_x$, $LiTaO_x$, $LiSiO_x$ and $LiPO_x$, that are potentially suitable coating materials.[33] In this respect, Sun's group initiated a great leap forward in the development of coating layers by ALD technique, all these materials can be deposited

by ALD technique as amorphous and continuous thin films with a controllable thickness (Figure 2).[44–48]

Self-limiting behavior and uniform growth at different compositions were achieved by varying the sub-cycle combinations of the ALD recipes. For example, by changing the ratio of Li to Nb subcycles in the ALD process, the electrochemical performance of $LiNbO_x$ film can be changed. With the Li/Nb subcycle ratio of 1 : 4, the lithium-ion conductivity of $LiNbO_x$ can reach 6×10^{-8} S/cm at room temperature (Figure 2a).[44] Similar to the ALD process of $LiNbO_x$, by using the same LiO^tBu precursor for Li–O in combination with other element-specific precursors, such as titanium isopropoxide (TTIP) for Ti, tantalum(V) ethoxide ($Ta(OEt)_5$) for Ta, tetraethylorthosilane (TEOS) for Si, and trimethylphosphate (TMPO) for P, the materials of $LiTiO_x$, $LiTaO_x$, $LiSiO_x$, and $LiPO_x$ can be deposited by ALD technique, respectively (Figure 2b–e).

4.2. Cathode interface modification in ASSLBs by ALD/MLD technique

We have selected several typical examples to show cathode interface modification in ASSLBs by ALD/MLD technique, as shown in Table 2. The early application was metal oxide materials. For instance, George et al.[42] did a coated Al_2O_3 layer (Figure 3a) on the surface of $LiCoO_2$ (LCO) particles and investigated the effects of Al_2O_3 on the interface between LCO and $Li_{3.15}Ge_{0.15}P_{0.85}S_4$. The EDS results show that Co, P, and S coexist at the interface and an interface layer is formed

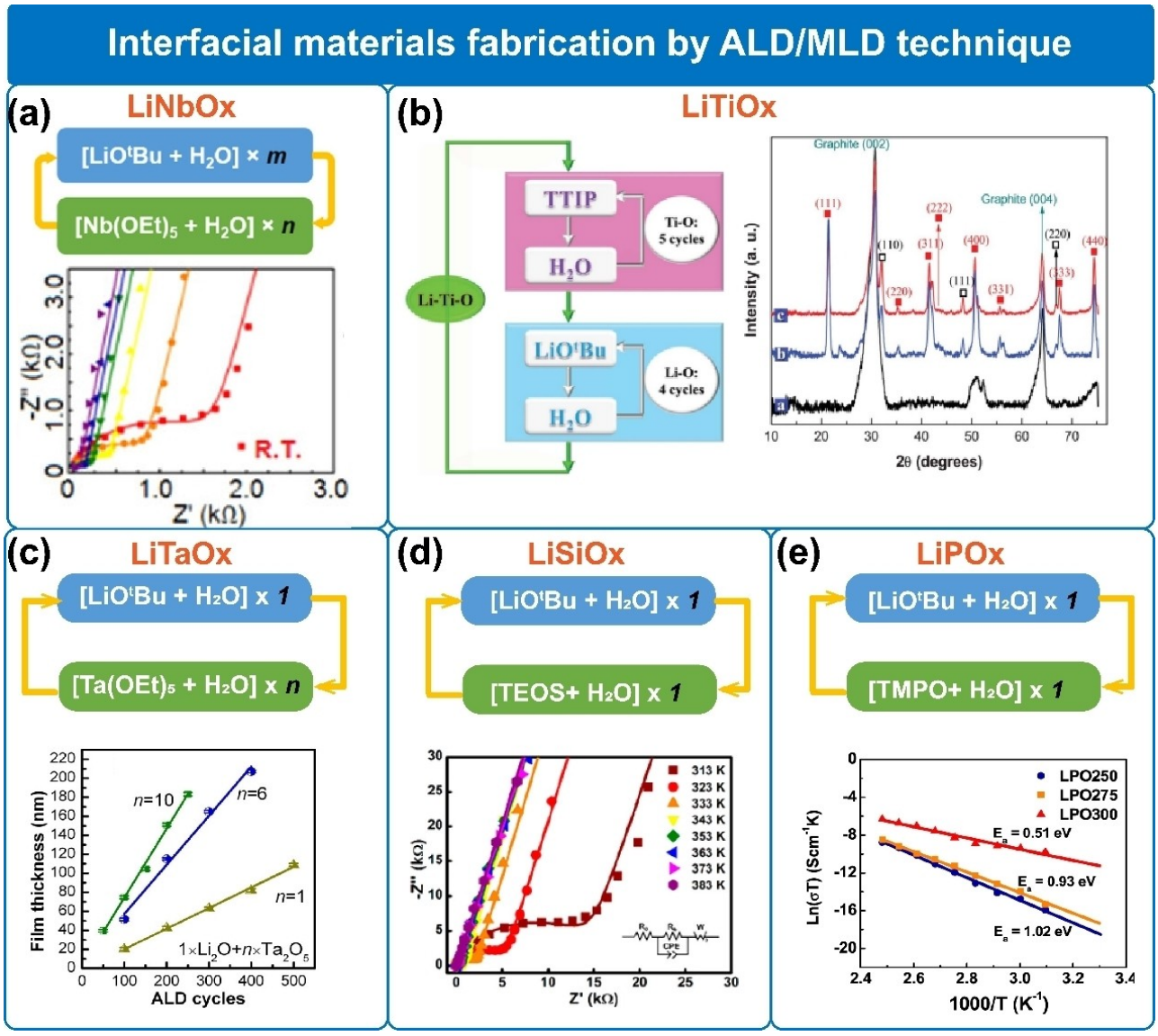

Figure 2. Interfacial materials fabrication by ALD/MLD technique. a) $LiNbO_x$. Reproduced with permission from Ref. [44]. Copyright (2018) American Chemical Society. b) $LiTiO_x$. Reproduced with permission from Ref. [45]. Copyright (2013) The Royal Society of Chemistry. c) $LiTaO_x$. Reproduced with permission from Ref. [46]. Copyright (2013) American Chemical Society. d) $LiSiO_x$. Reproduced with permission from Ref. [47]. Copyright (2017) American Chemical Society. e) $LiPO_x$. Reproduced with permission from Ref. [48]. Copyright (2015) American Institute of Physics.

Table 2. Typical surface coating on cathode electrode by ALD/MLD techniques in ASSLBs.

Substrate	ALD/MLD coating	Performance
$LiCoO_2$[42]	Al_2O_3	45 μA cm^{-2}, 3.3–4.3 V vs. Li^+/Li, 25th (90%)
$LiCoO_2$[49]	Li_2ZrO_3	2.52–4.22 V vs. Li^+/Li, 0.1 C, 100th (72%)
$LiNi_{0.8}Mn_{0.1}Co_{0.1}O_2$[50]	$LiNbO_3$	2.6–4.4 V vs. Li^+/Li, 0.1 C, 50th (99 mAh g^{-1})
$LiNi_{0.8}Mn_{0.1}Co_{0.1}O_2$[51]	PEDOT	2.7–4.4 V vs. Li^+/Li, 1 C, over 100 mAh g^{-1}
$LiNi_{0.8}Mn_{0.1}Co_{0.1}O_2$[52]	Li_3PO_4, 600 °C post-treatment	2.7–4.5 V vs. Li^+/Li, 0.1 C, 100th (77.9%)
$LiNi_{0.8}Mn_{0.1}Co_{0.1}O_2$[53]	$LiNbO_3$, 400 °C post-treatment	2.85–4.35 V vs. Li^+/Li, 1 C, 115 mAh g^{-1}
$LiNi_{0.85}Co_{0.10}Mn_{0.05}O_2$[54]	HfO_2, 400 °C post-treatment	2.90–4.30 V vs. Li^+/Li, 1 C, 60th (82%)

between LCO and SSE after cycling, corresponding to the multiple element's inter-diffusion. Moreover, the thickness of interface layer on bare LCO is ~30 nm while only ~17 nm for the Al_2O_3 coated sample, indicating that the Al_2O_3 coating by ALD can prevent the direct multi-elemental inter-diffusion between LCO and SSE and therefore inhibits interfacial side reactions.

However, traditional metal oxide coatings are not always effective in ASSLBs, especially in terms of interface element interdiffusion. Liu et al.[55] applied non-destructive variable-energy hard X-ray photoemission spectroscopy (VE-HAXPS) to unveil the elemental interdiffusion at the interface between LCO cathode and ($Li_{1.3}Al_{0.3}Ti_{1.7}(PO_4)_3$) LATP SSEs (Figure 3b) with and without the introduction of interlayer. Al_2O_3 and Li_3PO_4 are coated on the LATP SSEs by ALD technique, respectively. They are labeled as LATP-LCO, LATP- Al_2O_3-LCO, and LATP-Li_3PO_4-LCO samples. The VE-HAXPS spectra indicate the Al_2O_3 layer intensively diffuses into the LCO layer in LATP- Al_2O_3-LCO sample, instead of diffusion of LATP. In contrast, the diffusion of LATP could not be observed in the LATP-Li_3PO_4-LCO interface. The results indicate that Li_3PO_4 can efficiently prevent the elemental interdiffusion between the LCO and LATP, while Al_2O_3 cannot. Therefore, it is noteworthy to carefully develop suitable ALD coating layers according to actual battery systems.

In this respect, Sun's group realizes the deposition of a series of lithium-containing compounds such as Li_2ZrO_3 (LZO)[49] and $LiNbO_3$ (LNO)[50] on the layered oxide cathode material, i.e., $LiCoO_2$ (LCO) and $LiNi_{0.8}Mn_{0.1}Co_{0.1}O_2$ (NCM811) in the ASSLBs, respectively (Figure 3c and d). The ALD coating process of film is crucial for the electrochemical performance of the ASSLBs. By examining the ion conductivity of the LZO film deposited at 230 °C, 270 °C, and 300 °C, the ionic conductivity of LZO film reached 6.7×10^{-8} S/cm. The ALD LZO coating on LCO particles can prevent side reactions and provide Li^+ ion flux at the cathode interface, significantly improving the electrochemical performance of the LZO@ LCO cathode materials based ASSLBs (Figure 3c).

Among the various lithium-containing coating layer, $LiNbO_3$ has been established as the prototypical coating material in bulk ASSLBs because of its reasonable ionic conductivity and chemical/electrochemical stability against both layered oxide cathode and sulfide-based SSEs.[50,56,57] As shown in Figure 3(d), the operando XANES results show that bare NCM811 contact with LGPS induces parasitic reactions, and some LGPS are deposited to form Li_2S impurity phase. The introduction of the $LiNbO_3$ can stabilize the interface between Bare NCM and LGPS, avoiding the serious reaction between NCM 811 and LGPS and formation of side-products such as Li_2S.

Compared with ALD technique, MLD technique can deposit inorganic-organic composite layers and expand the types of coating material. However, current works lack discussion on the oxidation stability of organic coatings by MLD technique at high voltage, and therefore it has not been widely used yet. Sun's group attempts a uniform and conformal poly(3,4-ethylenedioxythiophene) (PEDOT) coating on both NCM811 and carbon additives (CNTs) via molecular layer deposition to reduce the effect of electron conductivity on the decomposition of SSEs (Figure 3e).[51] The PEDOT modification is designed as a P-type semiconductor, and it forms a metal/P-type semiconductor interface with CNTs. Therefore, the electronic conductivity of both PEDOT and CNTs is reduced. The PEDOT modified NCM811and CNTs ASSLB shows the specific capacity of over 100 mAh g^{-1} at 1 C, which is 10 times higher than that of uncoated ASSLB.

4.3. Post-treatment of the cathode modification by ALD/MLD technique

The above coating layer is generally direct deposited on the active materials without post-treatment, which usually undergo unfavorable structure or morphology changes after high-temperature anneals, such as shrinking into island-like structures.[58] Therefore, the coated material is directly used as the cathode of ASSLBs. However, recent studies show that the suitable annealing treatment could not only achieve the thin-film functional design, but also enhance the ionic conductivity of the ALD coating layer.

Sun et al.[52] explored that a deposition of lithium phosphate (LPO) coating on the surface of NCM811 by ALD technique and the materials are further annealed at 600 °C for 2 h. It is shown that the LPO penetrate into the grain boundary in bulk structure of NCM811 firstly. Then, while the LPO-annealed powders are re-covered with an LPO coating (Figure 4a). The LPO exists both on the surface and in the bulk structure of polycrystalline NCM811, not only alleviating side reactions but also suppressing the microstructural cracks of the cathode.

By combining the ALD technique and post-annealing, Liu and coworkers found that the initial discharge capacity of NCM811 electrode coated with $LiNbO_x$ coating layer could be increased to 205 mAh g^{-1} in the sulfide-based ASSLBs (Figure 4b).[53] Their experiments show that the modified $LiNbO_x$ layer becomes smoother and adheres tightly to NCM811

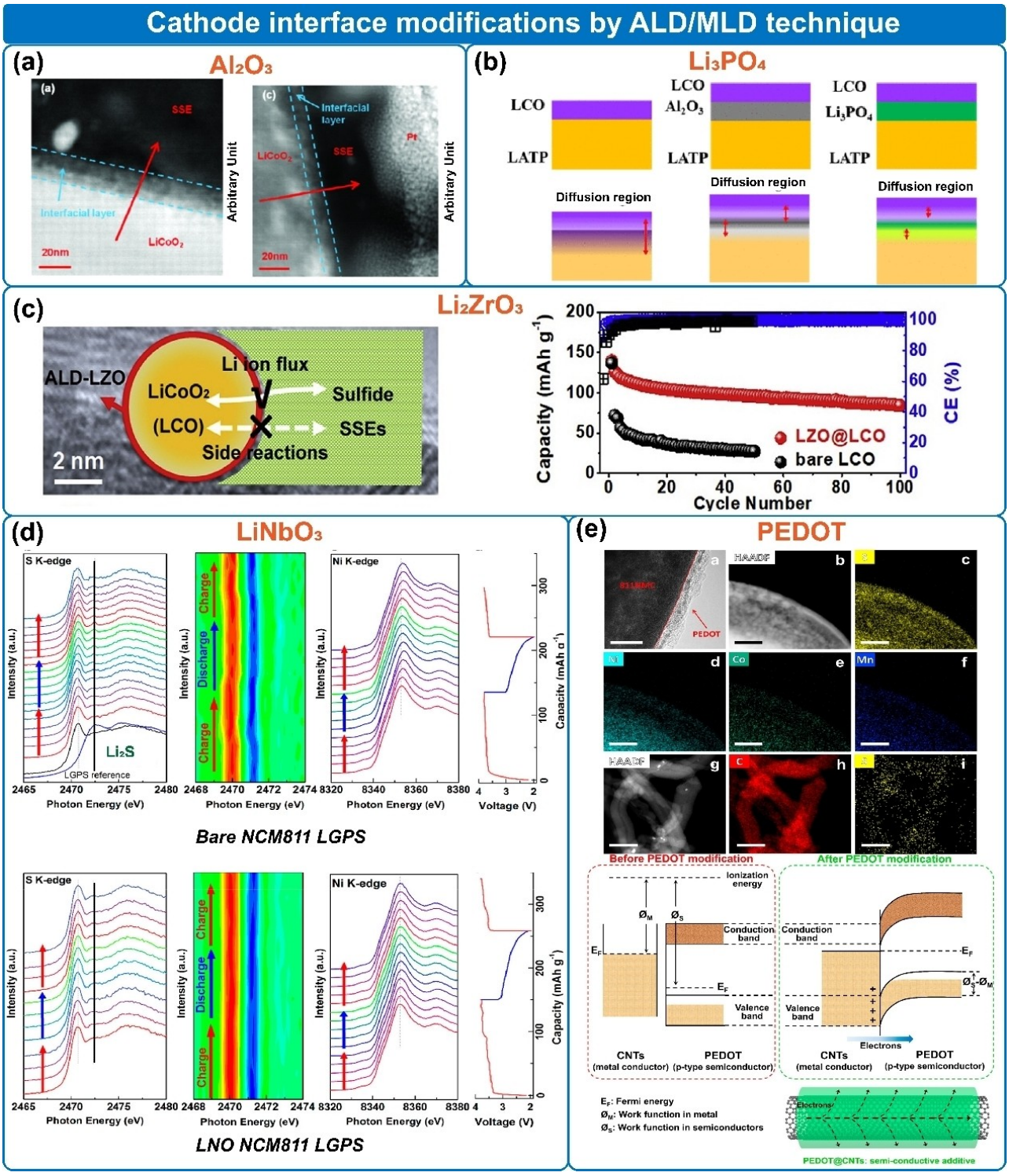

Figure 3. Modification films deposited by ALD/MLD methods for cathode application. a) Al_2O_3 films for $LiCoO_2/Li_{3.15}Ge_{0.15}P_{0.85}S_4$ SSE interface. Reproduced with permission from Ref. [42]. Copyright (2012) Electrochemical Society. b) Element diffusion at the interface of LATP-LCO, LATP-Al_2O_3-LCO, and LATP-Li_3PO_4-LCO. Reproduced with permission from Ref. [55]. Copyright (2020) American Chemical Society. c) Li_2ZrO_3 films for $LiCoO_2/Li_6PS_5Cl$ SSE interface. Reproduced with permission from Ref. [49]. Copyright (2020) Elsevier. d) Operando XANES results for bare NCM811-LGPS and NCM811-$LiNbO_3$-LGPS. Reproduced with permission from Ref. [50]. Copyright (2019) American Chemical Society. e) PEDOT films by MLD technique for NCM811 and CNTs. Reproduced with permission from Ref. [51]. Copyright (2020) American Chemical Society.

particles, exhibiting higher crystallinity and lithium-ion conductivity. In addition, the coating layers after post-annealing at low temperature normally exhibit higher crystallinity and thus higher ionic conductivity. On the contrary, the crystallinity of some ALD coatings will decrease during the post-annealing treatment. David et al.[54] carried out the ALD technique to coat

Concept
doi.org/10.1002/batt.202200359
Chemistry Europe
European Chemical Societies Publishing

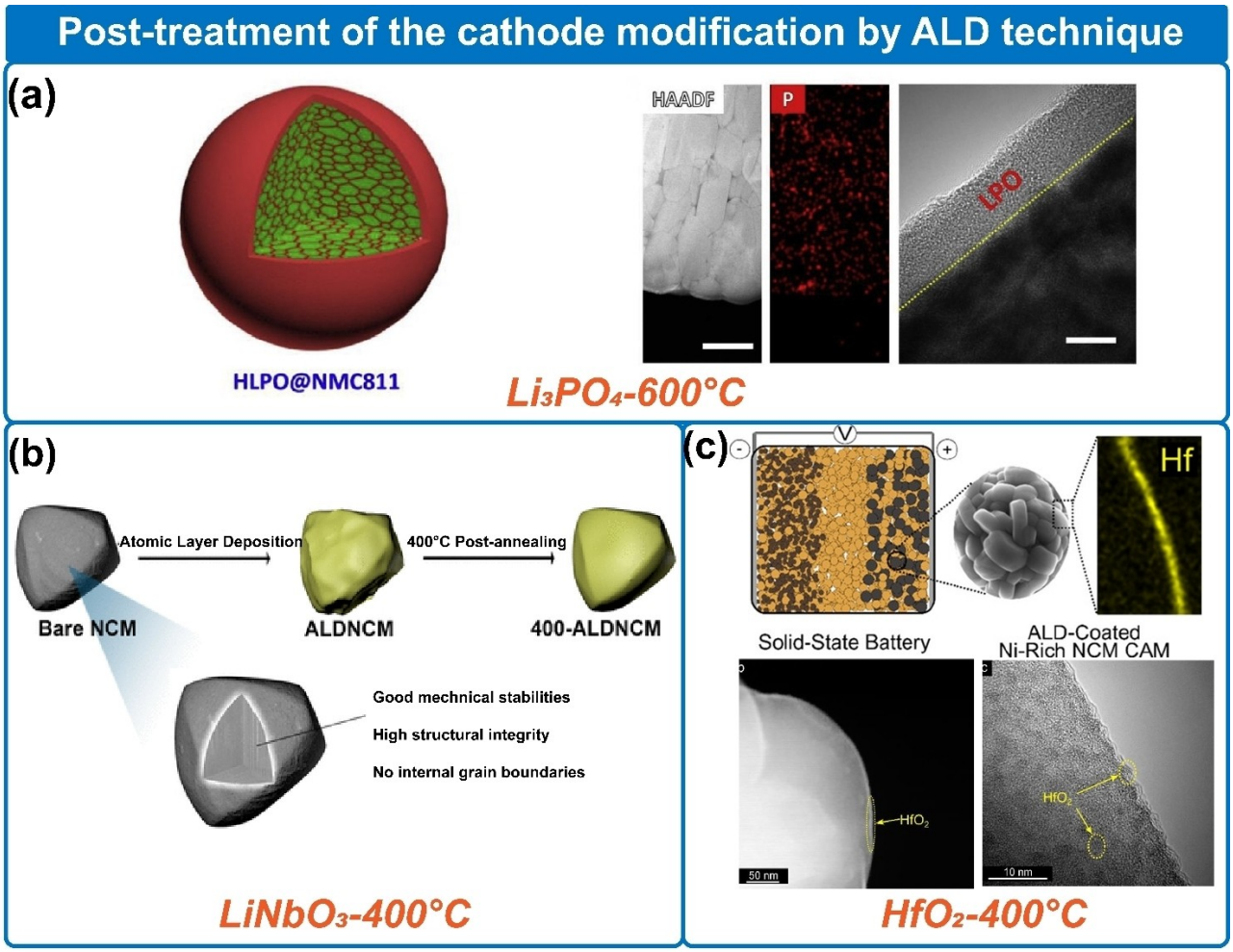

Figure 4. Post-treatments of ALD deposited films for cathode application. a) lithium phosphate (LPO) treated at 600 °C; Reproduced with permission from Ref. [52]. Copyright (2020) Elsevier. b) $LiNbO_3$ treated at 400 °C; Reproduced with permission from Ref. [53]. Copyright (2021) American Chemical Society. c) HfO_2 treated at 400 °C; Reproduced with permission from Ref. [54]. Copyright (2021) American Chemical Society.

the HfO_2 coating on the surface of $LiNi_{0.85}Co_{0.10}Mn_{0.05}O_2$ particles (Figure 4c). The TEM results show some nanocrystalline regions in the HfO_2 layer after being deposited by ALD, while a smooth amorphous coating is formed after post-annealed at 400 °C with O_2 atmosphere. They believe that HfO_2 coating should react with the residual lithium compounds on the surface of substrate material to form the lithium-containing ternary oxide, which is beneficial to the electrochemical performance of the NCM materials. However, the mechanism of high-temperature treatment coating for improving battery electro performance needs further study from bulk to surface by advanced characterization.

5. Surface Coating on the Lithium Metal Anode

Lithium metal anode is receiving great attention for its high theoretical capacity of 3860 mAh g^{-1} and low redox potential. It is recognized that the prerequisite for achieving high energy in ASSLBs is the use of lithium metal anode.[26] However, when lithium metal anode is practically applied in bulk-type ASSLBs, we need to consider the following issues:

i) Interfacial chemical/electrochemical reactions. Most SSEs are unstable and decomposed into the low-valence compound when contacted with Li. The formation of an unstable interface limits the Li^+ transfer between SSEs and Li metal, resulting in a large interface impedance.
ii) The formation and growth of Lithium dendrite. Due to the physical contact failure, lithium metal, or electrolyte defects, lithium is frequently deposited unevenly on the lithium metal anode firstly, resulting in the growth of lithium dendrites between Li and solid electrolytes and even penetrates the solid electrolytes.
iii) Physical contact issues between electrolytes and Li metal. Repeated deposition and stripping of lithium metal anode lead to significant volumetric changes of the Li electrode, and the formation of voids between electrolyte and lithium metal, especially when using thick Li foils.

The controllable, flexible and uniform thin surface coating deposited by ALD/MLD techniques is considered to be able to partially overcome the above-mentioned problems.

5.1. Suppressing the interfacial side reactions

To prevent the chemical reactions and stabilize the interface between $Li_{6.75}La_{2.75}Ca_{0.25}Zr_{1.75}Nb_{0.25}O_{12}$ and lithium metal anode, Hu et al.[59] deposited Al_2O_3 layer on $Li_{6.75}La_{2.75}Ca_{0.25}Zr_{1.75}Nb_{0.25}O_{12}$, which show a stable interface toward Li metal (Figure 5a). The Al_2O_3 coated $Li_{6.75}La_{2.75}Ca_{0.25}Zr_{1.75}Nb_{0.25}O_{12}$ can not only inhibit the interface side reaction but also keep a durable contact with lithium metal anode.

Similarly, Sun et al.[60] further confirmed the similar effects of the Al_2O_3 coating layer. They proposed that the Al_2O_3 coating could transform into a lithium-ion conductivity layer of Li–Al–O during cycling, which reduced the interface impedance. It is also shown that Al_2O_3 coating effectively prevents the side reaction between lithium metal and LATP (Figure 5b). In addition, Sun et al.[61] also prepared an organic-inorganic mixed intermediate layer (alucone layer) by MLD at the $Li_{10}SnP_2S_{12}$/lithium metal interface. The alucone layer significantly suppresses the reduction of Sn^{4+} by Li metal, suggesting an effective inhibition of interfacial side reactions.

5.2. Preventing the Li dendrites formation

A bifunctional alucone layer prepared on Li metal by MLD not only inhibits the side reactions between Li and electrolytes but also could limit the formation of lithium dendrites (Figure 5c).[61] Specifically, the Li symmetric cells with the coated SSE exhibit a low over-potential of Li plating/stripping which is less than 0.5 V within 10000 minutes at the current density of 0.1 mA cm^{-2}, while the lithium metal anode with bare SSE show significantly larger over potential after 4000 minutes, and the short-circuit happened at this time. Recently, the hexagonal

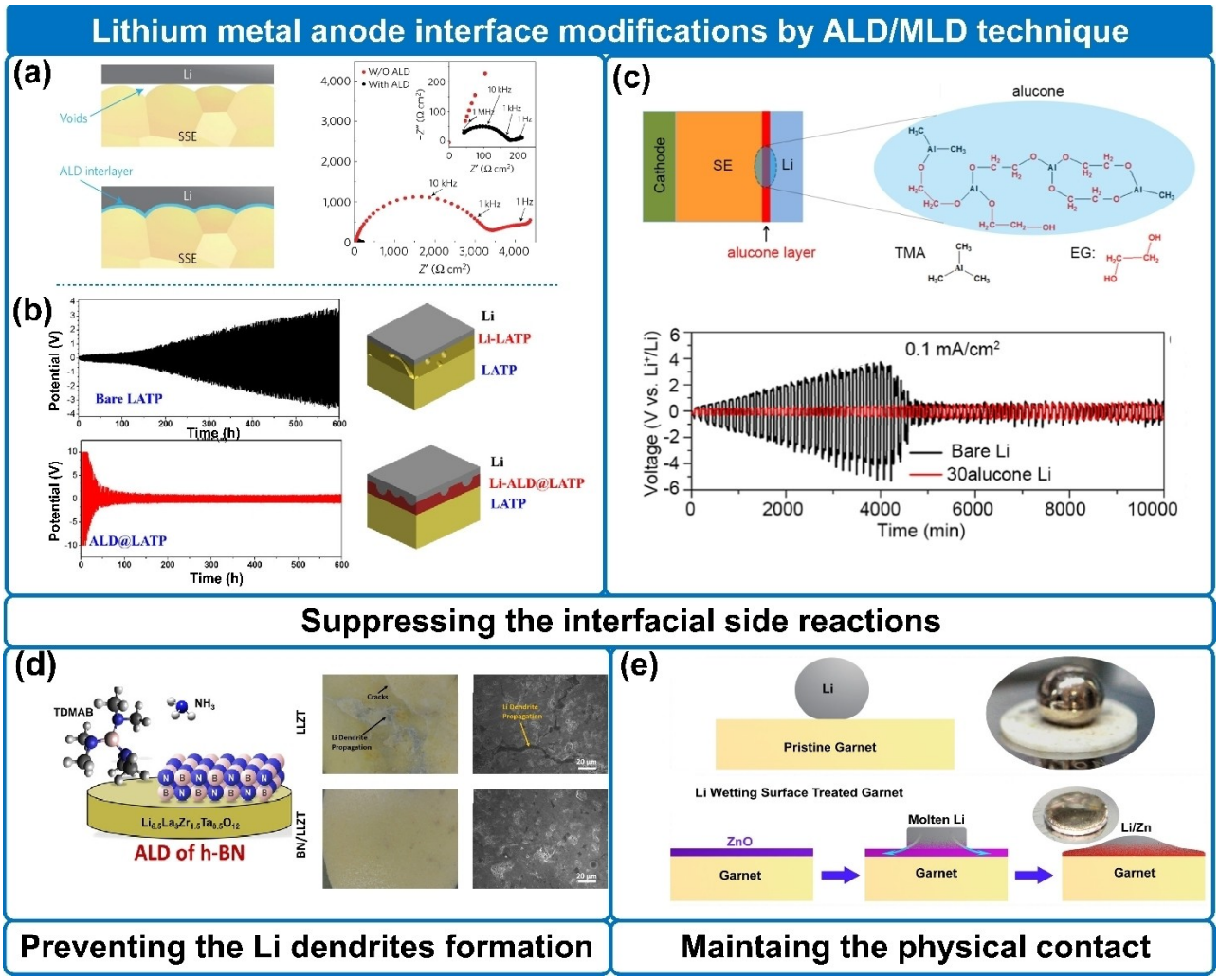

Figure 5. a) Solving the interfacial issue between Li metal anode and garnet-type $Li_{6.75}La_{2.75}Ca_{0.25}Zr_{1.75}Nb_{0.25}O_{12}$ by ALD Al_2O_3 coating. Reproduced with permission from Ref. [59]. Copyright (2016) Nature Publishing Group. b) The application of the ALD Al_2O_3 coating on LATP electrolyte to stabilize LATP/Li metal interface. Reproduced with permission from Ref. [60]. Copyright (2018) American Chemistry Society. c) The use of MLD to develop an alucone layer at the interface between the Li metal and $Li_{10}SnP_2S_{12}$. Reproduced with permission from Ref. [61]. Copyright (2018) Elsevier. d) Preventing the Li dendrites formation between the Li and LLZT by ALD h-BN coating. Reproduced with permission from Ref. [62]. Copyright (2021) American Chemistry Society. e) Improving the wettability of the garnet electrolyte for molten lithium by ALD ZnO coating. Reproduced with permission from Ref. [63]. Copyright (2016) American Chemistry Society.

boron nitride (h-BN) is deposited on both sides of the $Li_{6.5}La_3Zr_{1.5}Ta_{0.5}O_{12}$ pellets by ALD to suppress the propagation of lithium dendrites.[62] The h-BN layers can prevent electron tunneling across the interface and create uniform Li-ion fluxes to promote homogeneous deposition of metallic Li (Figure 5d).

5.3. Maintaining the physical contacts between SSEs and lithium metal anodes

The poor wettability of garnet solid electrolyte to lithium leads to poor contact between garnet solid electrolyte and lithium metal, resulting in large electrochemical polarization, uneven ion flow through the interface, and high interface impedance. In addition, large volumetric changes of lithium metal during cycling and the rigidity of the garnet electrolyte also lead to poor contact between SSE and lithium metal. To conquer these issues, Hu et al.[63] did a coating of ZnO on $Li_7La_3Zr_2O_{12}$ by ALD, which enhances the compatibility between lithium metal and $Li_7La_3Zr_2O_{12}$ (Figure 5e). Similarly, through ALD technique, the Al_2O_3 coated $Li_{6.75}La_{2.75}Ca_{0.25}Zr_{1.75}Nb_{0.25}O_{12}$ can not only inhibit the interface side reaction but also keep a durable contact with lithium metal anode (Figure 5c).[59]

As described above, the coating layer deposited by ALD/MLD technique shows obvious strengths in terms of suppressing the interfacial side reaction, preventing the growth of lithium dendrite and maintaining good physical contact between lithium metal anode and SSEs. The reason for the beneficial effect on the lithium metal anode is that ALD/MLD technique can precisely control the thickness and uniformity of the coating layer, and it can operate at low temperature, which is especially suitable for the substrates with low melting point and poor thermal stability, such as lithium metal (e.g., pure Li melting point is about 180 °C). However, there are few studies on the interface modification for lithium metal anode by ALD/MLD, it is anticipated that well-controlled MLD techniques could be explored for the construction of artificial SEI on Li metal for future research.

6. The Application of ALD/MLD in 2D and 3D Thin-Film ASSLBs

Thin-film ASSLB is one of the most attractive battery systems owing to their high safety, versatility, and flexibility, it has been widely used in implanted medical equipment, wireless microsensors, micro-electro-mechanical system equipment, flexible electronics, etc.[64,65] The typical structure of two-dimensional (2D) thin-film ASSLBs belongs to the sandwich configuration, which is composed of the cathode film, solid-state electrolyte film and anode film (e.g., the metallic lithium and alloys). However, 2D thin-film ASSLBs are limited in terms of energy output.[66] A feasible approach to increase the energy density of 2D thin-film ASSLBs is to increase the thickness of electrodes, while the power density will compromise. The demands on high power and energy density promote the development of 3D micro-ASSLBs, which have a much higher specific surface that allows usage of more active materials in the same footprint area, and short diffusion path. New challenges of 3D micro-ASSLBs lie in the deposition of conformal and dense thin films onto narrow battery assemblies. In this respect, ALD/MLD techniques have tremendous advantages that can offer exquisite thickness control and adjustable stoichiometric composition on complex substrates such as 3D high aspect-ratio structures.[27] Due to the above advantages, the application of ALD/MLD in fabricating key battery components (the cathode, anode, and solid-state electrolytes) has been intensively investigated in 2D and 3D thin-film ASSLBs.

6.1. Electrode Fabrication

In general, the cathode is the key component that limits the practical performance such as the energy density of the battery, so it is necessary to carefully select suitable cathode materials to achieve high performance thin-film ASSLBs. Lithium-free materials were first used as the cathode materials in thin-film micro-ASSLBs, including TiS_2,[67] MoO_3[68] and V_2O_5,[69] etc. Unfortunately, these types of cathode films exhibit low working potential and poor cycling performance. Subsequently, deposition of a series of lithium-containing cathode materials such as $LiCoO_2$, $LiMn_2O_4$, and $LiFePO_4$ were also explored by ALD techniques. Due to the high working potential, good rate capacity, and long cycle life, $LiCoO_2$ has dominated the market of portable electronic equipment in the past few decades. Similarly, $LiCoO_2$ film deposited by ALD technique also acted lithium-containing cathode in thin-film ASSLBs. For example, Donders et al.[70] developed a remote plasma ALD process for preparing $LiCoO_2$ thin films, which consist of the two individual ALD process for the Co_3O_4 and Li_2CO_3, by using $CoCp_2$ as the cobalt source, LiO^tBu as the lithium source, O_2 plasma as the oxidation source (Figure 6a). Their results showed that the specific capacity of $LiCoO_2$ thin film is dependent on the ALD dosing ratio after annealing at 700 °C for 6 minutes. In the case of Co: Li dosing ratio x of 4, the maximum theoretical storage capacity was obtained (Figure 7a).

Many other lithium-containing cathodes, including $Li_xMn_2O_4$ and $LiFePO_4$, can be prepared by using a similar deposition approach, combining Li_2O subcycle with another one or two binary oxides ALD subcycles. For instance, Miikkulainen et al.[71] synthesized polycrystalline $Li_xMn_2O_4$ by combining the oxidation of $(Mn(EtCp)_2/O_3)$ process with Li(thd) $(LiN(SiMe_3)_2)/O_3$ at 225 °C (Figure 6b). The $Li_xMn_2O_4$ films present high specific capacity and good cycling stability (Figure 7b), which make it attractive for application in thin-film 3D micro-ASSLBs. Recently, Sheil et al.[74] reported a plasma enhanced atomic layer deposition (PEALD) process for $Li_{1+x}Mn_{2-x}O_4$ ($x \leq 0.33$), and a 3D micro-battery consisting of $Li_{1+x}Mn_{2-x}O_4$ cathode layer, $Li_xAl_ySi_zO$ solid electrolyte deposited by ALD and SiGe nanowire anode was assembled. The $Li_{1+x}Mn_{2-x}O_4$ thin film exhibited great rate capability and capacity retention with ~97% capacity retention over 100 cycles at 36 $\mu A\,cm^{-2}$ (~5 C) between 3.5–4.5 V vs. Li/Li^+.

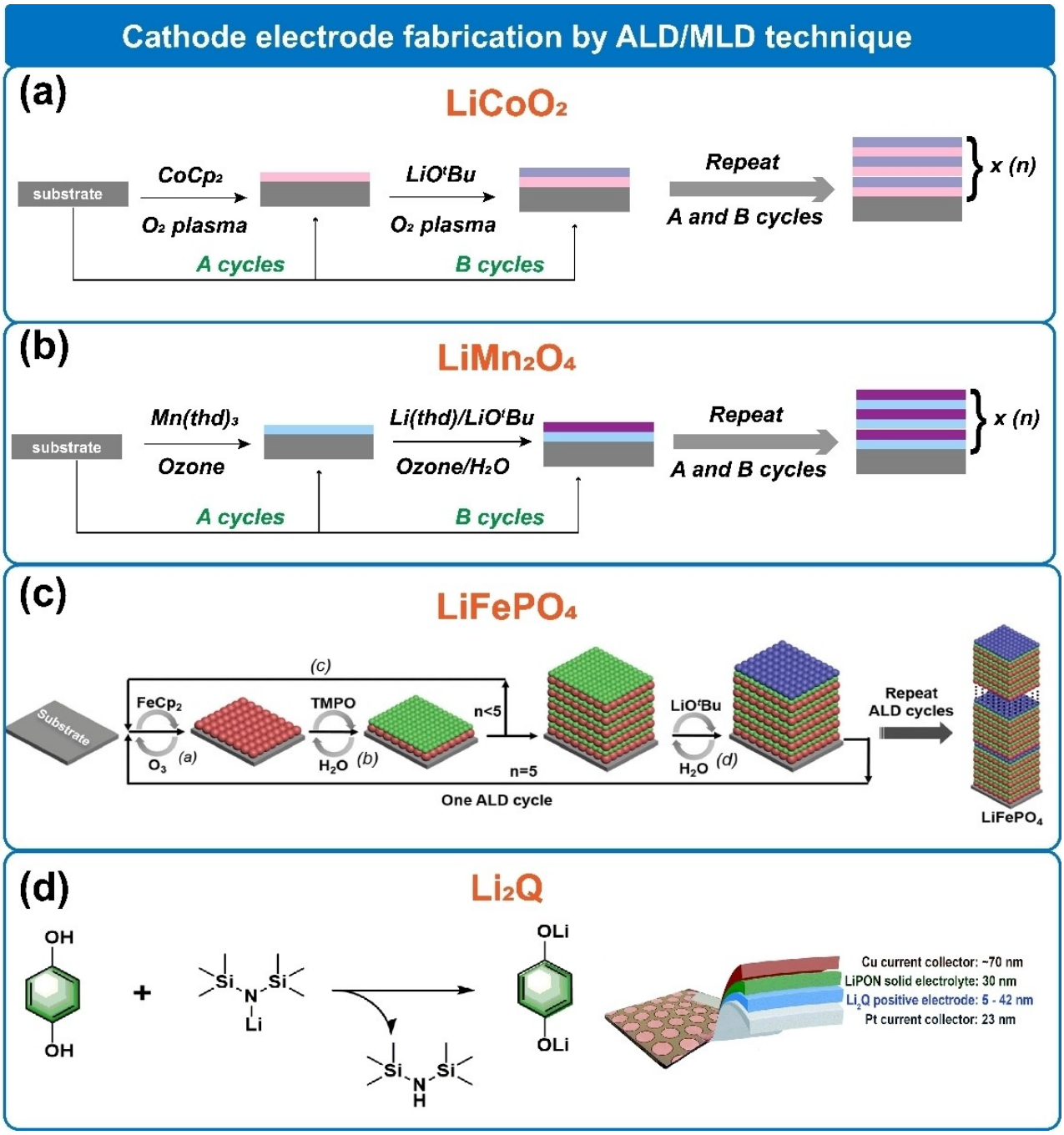

Figure 6. Cathode electrode fabrication by ALD/MLD technique. a) $LiCoO_2$. Reproduced with permission from Ref. [70]. Copyright (2013) IOP Publishing. b) $LiMn_2O_4$. Reproduced with permission from Ref. [71]. Copyright (2014) American Chemical Society. c) $LiFePO_4$. Reproduced with permission from Ref. [72]. Copyright (2014) Wiley-VCH. d) Li_2Q (dilithium-1,4-benzenediolate). Reproduced with permission from Ref. [73]. Copyright (2018) The Royal Society of Chemistry.

Compared to the binary and ternary cathode materials, it is more challenging to deposit quaternary materials by using ALD technique. Sun's group successfully synthesized $LiFePO_4$/CNT composite electrode material on the carbon nanotube substrate by ALD for the first time (Figure 6c).[72] The ALD deposition process $LiFePO_4$ consists of 5 subcycles of (Fe_2O_3 + PO_x) and 1 subcycle of Li_2O. After the post-annealing treatment, amorphous $LiFePO_4$ transforms into a polycrystalline state. The conductive network of Fe_3P impurities is considered to be the reason for the excellent rate performance of $LiFePO_4$/CNT composite electrode (Figure 7c), which is formed by carbothermal reduction of $LiFePO_4$ when the residual organic ligands are annealed in Ar gas and carbon nanotubes.

In addition, the research of various new organic thin films with good electrochemical activity has made significant progress in the last several years. For example, Nisula et al employed Li(thd) (thd = 2,2,6,6-tetramethyl-3,5-heptane-dione) as metal precursor and different organic precursor developed a

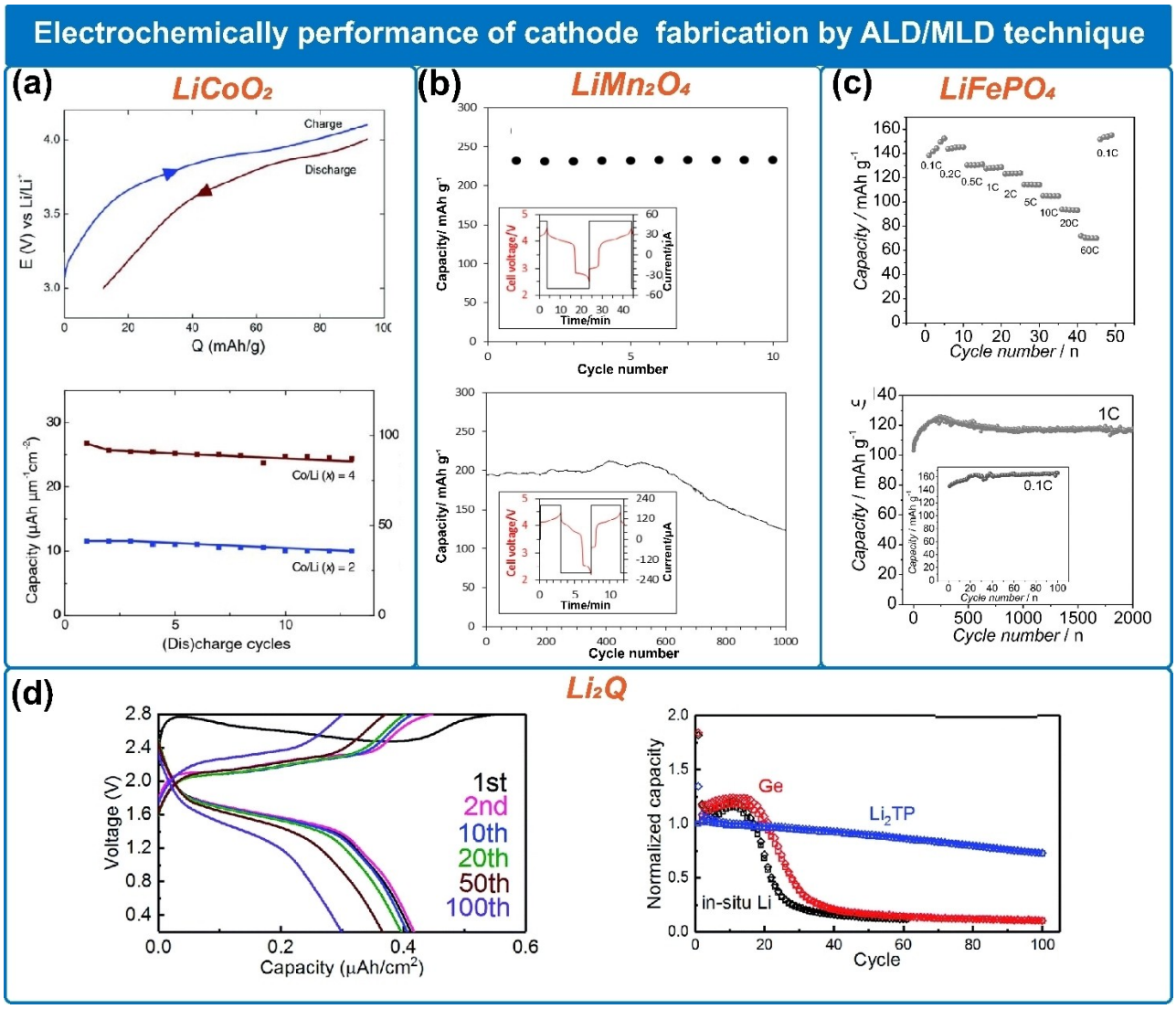

Figure 7. Electrochemically performance of cathode electrode fabrication by ALD/MLD technique. a) $LiCoO_2$. Reproduced with permission from Ref. [70]. Copyright (2013) IOP Publishing. b) $LiMn_2O_4$. Reproduced with permission from Ref. [71]. Copyright (2014) American Chemical Society. c) $LiFePO_4$. Reproduced with permission from Ref. [72]. Copyright (2014) Wiley-VCH. d) Li_2Q (dilithium-1,4-benzenediolate). Reproduced with permission from Ref. [73]. Copyright (2018) The Royal Society of Chemistry.

series of electrochemically active lithium-organic films as electrodes, such as Li-TP or Li-TPA (lithium terephthalate),[75,76] Li_2TP-NH_2 (dilithium 2-aminoterephthalate),[76] Li-NDC (lithium 2,6-naphthalenedicarboxylate), Li-BPDC (lithium 4,4′-biphenyldicarboxylate), Li-PDC (lithium pyridinedicarboxylate), and Li-AZO (lithium 4,4′-azobenzene-dicarboxylate)[77] have been investigated. The crystal structure of these lithium-organic films experiences minimal changes during metal ion intercalation/deintercalation making these materials particularly suitable for wearable electronics. Most notably, Nisula et al.[73] used (lithium bis-(trimethylsilyl) amide (LiHMDS) and (hydroquinone) HQ deposited Li_2Q was used as the cathode material (Figure 6d). Compared with traditional quinone-based organic electrode materials (such as p-benzoquinone), Li_2Q films by MLD technique can do in-situ lithiation, and thus can be directly used as cathode materials in the as-prepared micro-battery. The Li_2Q film cathodes also exhibit ultrahigh rate capability without any conductive additives. In Li_2Q/LiPON/Cu batteries, it can reach 50% of the full capacity in 0.25 s. Nisula et al.[73] also constructed successfully Li_2Q/LiPON/Li-TPA (lithium terephthalate) organic batteries by using ALD/MLD techniques, demonstrating the application potential of ALD/MLD technique to complete the entire preparation of the full organic thin-film batteries (Figure 7d).

6.2. Solid Electrolyte Fabrication

Compared with conventional SSEs synthesis methods, ALD/MLD techniques can adjust easily the lithium-ion conductivity, electrochemical window, and mechanical strength of thin-film SSEs through the careful design of thin-film composition and structure. In particular, ALD/MLD techniques can deposit highly conformal layers with atomic precision on high aspect-ratio

substrates. Given these remarkable characteristics, it is very encouraging to implement ALD/MLD to synthesize and manufacture different configurations of SSEs with ideal properties for thin-film ASSLBs.

Many types of solid electrolytes such as LIPON, garnet, oxide, sulfide, phosphate, perovskite, (Li_3BO_3-Li_2CO_3) LBCO, and lithium-containing organic thin-film electrolytes have been synthesized by using ALD/MLD techniques.[78,79] To obtain target solid electrolytes with ideal electrochemical performance, it is necessary to select suitable precursors and operating conditions.[29] In the Table 3, we list the different types of SSEs synthesized by ALD/MLD technique and summarize the ALD/MLD deposition temperature and the precursors, as well as the growth thickness per cycle (GPC) and ion conductivity of the film.

As shown in Table 3, the lithium-ion conductivity of the amorphous thin film electrolyte deposited by ALD/MLD ranges from 10^{-9} to 10^{-7} S cm^{-1} at room temperature, which cannot completely meet the needs of high performance thin-film micro-ASSLBs. Therefore, it is necessary to increase the lithium-ion conductivity of deposited films. The ion conductivity of Li_3BO_3-Li_2CO_3 has already reached 6.0×10^{-7} S cm^{-1} (at room temperature) when it was first reported coating on $LiCoO_2$ for sulfide-based ASSLBs by solution process.[90]

By using lithium tert-butoxide (LiO^tBu) as the lithium source, $[(CH_3)_2CHO]_3B$ (TIB) as the boron source, and Ozone as the oxidant, Kazyak et al.[87] reported that as prepared Li_3BO_3-Li_2CO_3 (LBCO) film has an ionic conductivity of 10^{-6} S cm^{-1} at room temperature by ALD technique. By regulating the ratio of carbon to boron in the film can achieve a higher ionic conductivity, i.e., the higher Li_2CO_3 content, the higher Li^+ mobility of the film. Both of the experiments and theoretical calculation results show that the coordination environment of the B atom would change with the addition of Li_2O in the system, causing the depolymerization structure with the bridging oxygen (BO) groups to be transformed into the non-bridging oxygen (NBO) structure. More open structures and NBO-rich regions will facilitate lithium ion diffusion. Furthermore, AIMD (ad initio molecular dynamics) simulations of Li_3BO_3 (LBO) and Li_3BO_3-Li_2CO_3 (LBCO) illustrate the presence of carbonate increases the mobility of O coordinated with C or B. Thus, Li_3BO_3-Li_2CO_3 deposited at 200 °C exhibits a high ionic conductivity at RT of 2.23×10^{-6} S cm^{-1}.

LiPON (lithium phosphorus oxynitride) has been one of the most popular solid-state electrolytes used for lithium ion microbatteries. By adjusting the N to P ratios in the films, the ionic conductivity of LiPON can be increased.[91] Karppinen et al.[81] used LIHMDS and DEPA as precursors to deposit LiPON thin film. The ALD process can employ nitrogen-containing phosphorus precursors to transfer the P–N bond into the LiPON films. The ionic conductivity of $Li_{0.96}PO_3N_{0.60}$ films deposited at 330 °C can be achieved as 6.6×10^{-7} S cm^{-1} at room temperature. In addition, the morphology of LiPON can be changed during the ALD process. Gary et al.[80] show the effect of the nitrogen content on the morphology of the LiPON film by using N_2 plasma during the ALD process. As the N content increases, ALD LiPON films transition from polycrystalline to amorphous and ionic conductivity of LiPON also increases up to 3.0×10^{-7} S cm^{-1}.

In combining organometallic with organic precursors, MLD could synthesize a new type of flexible lithium-containing organic thin-film SSEs. For example, Wang et al.[88] used LiO^tBu and 1,3-propanediol to deposit lithium propane dioxide ($Li_2O_2C_3H_6$, LPDO), which exhibited the deposited rate of 0.23 Å/cycle and 0.15 Å/cycle at 150 °C and 200 °C, respectively. In addition, Kazyak et al.[89] firstly used LiO^tBu and ethylene glycol to synthesize lithicone. After post-annealing at 350 °C, the lithicone film exhibits the ionic conductivity of 3.6×10^{-8} S cm^{-1}

Table 3. Li-ion containing solid-state electrolyte synthesized via ALD/MLD techniques.

Compounds		Deposition temperature [°C]	ALD/MLD precursors	Ionic conductivity [S cm^{-1}]	GPC [Å per cycle]
LIPON	$Li_{0.99}PO_{2.55}N_{0.30}$[80]	250	LiO^tBu/H_2O/TMP[a]/plasma N_2	3.0×10^{-7}(RT)	1.05
	$Li_{0.95}PO_{3.00}N_{0.60}$[81]	270–310	LiHMD/DEPA[b]	6.6×10^{-7}(RT)	0.7
	Li_2PO_2N[82]	200,300	LiO^tBu/DEPA	$6.51\pm0.36\times10^{-7}$(35 °C) $3.7\pm0.2\times10^{-7}$(RT)	0.15,0.9
	Li_2PO_2N[83]	250	LiO^tBu/DEPA	–	0.6
Garnet	Al-doped $Li_7La_3Zr_3O_{12}$[58]	200	LiO^tBu/LaFAMD[c]/TDMAZ[d]/TMA	1×10^{-8}(25 °C) 7.8×10^{-5}(200 °C)	–
Oxide	$Li_{5.1}TaO_z$[45]	225	LiO^tBu/Ta $(OC_2H_5)_5$/H_2O	2×10^{-8}(26 °C)	2.1
	$LiNbO_x$[43]	235	LiO^tBu/[Nb $(OEt)_5$]/H_2O	6.39×10^{-8}(30 °C)	–
	Li_xSiO[46]	250	LiO^tBu/TEOS/H_2O	5.72×10^{-9}(30 °C)	0.80–1.36
	$Li_xAl_ySi_zO$[84]	290	LiO^tBu/TMA/TEOS/H_2O	10^{-7} to 10^{-9}(RT)	–
Phosphate	$Li_{2.8}PO_z$[47]	250–325	LiO^tBu/TMPO	3.3×10^{-8}(26 °C)	0.57–0.74
Perovskite	$Li_{0.32}La_{0.30}TiO_z$[85]	225	La$(thd)_3$/$TiCl_4$ /LiO^tBu/H_2O/O_3	–	0.48
Sulfide	Li_xAl_yS[86]	150	LiO^tBu/TMAD-Al[e]/H_2S	2.5×10^{-7}(RT)	0.50
LBCO	Li_3BO_3-Li_2CO_3[87]	200,260	LiO^tBu/TIB[f]/O_3	2.23×10^{-6}(25 °C)	0.65
Lithium-containing organic electrolyte	LPDO[88]	140–220	LiO^tBu/PD[g]	–	0.2–0.84
	Lithicone[89]	135,175	LiO^tBu/EG	3.6×10^{-8}(30 °C) 5×10^{-8} (30 °C)	2.6

[a] trimethylphosphate; [b] diethyl phosphoramidate; [c] tris (N, N′-diisopropylformamidinato) lanthanum; [d] tetrakis(dimethylamido) zirconium; [e] tris(dimethylamido) aluminum (III); [f] triisopropyl borate; [g] propanediol.

and 5×10^{-8} S cm^{-1} deposited at 175 °C and 135 °C, respectively. Although lithium-containing organic electrolytes have not been widely used in thin-film micro-ASSLBs, the current MLD technique makes it feasible which some kind of organic electrolytes could be used as a building block to incorporate with other precursors to tune their mechanical and electrochemical properties finely, we could anticipate that incorporation of organic blocks in the films should have enormous potential to build flexible interfacial layers in ASSLBs.

In summary, ALD/MLD technique can deposit various active materials as electrodes and electrolytes for thin-film solid-state batteries. Particularly, Pearse et al.[83] showed a 3D full micro-ASSLBs in which all active battery components (electrode, solid electrolyte, and current collectors) were deposited by ALD technique onto the silicon wafers with arrays of deep pores, demonstrating the exceptional ability of ALD/MLD to prepare the entire thin-film micro-ASSLBs.

7. Summary and Outlook

In this review, we overview the latest progress in the application of ALD/MLD in both bulk-type and thin-film-type micro-ASSLBs, including the atomic/molecular surface modification of the electrodes for bulk-type ASSLBs, and rational preparation of electrode and electrolyte materials for thin-film type ASSLBs. As far as we know, the interfacial stability between SSEs and electrodes significantly affects the electrochemical performance of bulk ASSLBs. By using ALD/MLD techniques, it is able to finely adjust the composition and thickness of the coating layers on the electrodes at the atomic/molecular level for interfacial controlling of the electrodes. Compared with uncoated cathodes, coated electrodes by ALD/MLD techniques have shown enhanced electro-chemo-mechanical compatibility with different solid electrolytes either in cathode or anode sides, especially for the sensitive sulfide-based electrolytes. It should be ideal to develop the coatings with wide electrochemical windows, high ionic conductivity and good mechanical properties in ASSLBs. In this direction, high-throughput computing may be a viable approach.

Besides, ALD/MLD techniques are versatile tools for the preparation of electrode and electrolyte materials of thin-film-type ASSLBs. For example, it is reported that the Li^+ ionic conductivity of solid electrolytes prepared by ALD/MLD technique can reach up to 10^{-6} S cm^{-1} at room temperature. Combining organometallic with organic precursors, it could make new organic or inorganic/organic composite electrolytes with reasonable ionic conductivity for thin-film-type ASSLBs. This field will attract more researchers to explore in the future. In this regard, many new inorganics or organic precursors for ALD/MLD process should be synthesized and developed by a collaboration between the organic chemist and material scientists.

On the other hand, the functionality and working mechanisms of ALD/MLD films in ASSLBs need further investigations. Advanced spectroscopic/imaging characterization methods, especially in situ spectroscopic/imaging techniques such as X-ray absorption spectroscopy/X-ray computed tomography (e.g., XAS/X-CT), high-resolution electron transmission microscopy (STEM) techniques, etc. can provide an in-depth understanding of the interfacial processes during cycling of the batteries, which can guide researchers to choose or optimize coating layers according to the specific demands of electrode materials.

In conclusion, ALD/MLD techniques provide a powerful deposition tool for making uniform and adjustable thin film with different functionality such as flexible and high ionic conductivity, etc., and it is also demonstrated that is an efficient and convenient method to enhance the electrochemical performance of ASSLBs. Although various thin-film materials and many useful interfacial strategies have been realized by ALD/MLD, the application of ALD/MLD in ASSLBs system still has great potential in terms of the synthesis of new precursors, elegant modification methods and scale-up applications.

Acknowledgements

This work was financially supported by National Key Research and Development Program of China (grant nos. 2021YFB2401800, 2018YFB0905400), National Natural Science Foundation of China (grant nos. 21935009, 21761132030).

Conflict of Interest

The authors declare no conflict of interest.

Keywords: all-solid-state batteries · atomic layer deposition · bulk solid-state batteries · molecular layer deposition · thin-film solid-state batteries

[1] S. Xia, X. Wu, Z. Zhang, Y. Cui, W. Liu, *Chem* **2019**, *5*, 753–785.
[2] A. Manthiram, X. Yu, S. Wang, *Nat. Rev. Mater.* **2017**, *2*, 16103.
[3] S. Randau, D. A. Weber, O. Koetz, R. Koerver, P. Braun, A. Weber, E. Ivers-Tiffee, T. Adermann, J. Kulisch, W. G. Zeier, F. H. Richter, J. Janek, *Nat. Energy.* **2020**, *5*, 259–270.
[4] E. Quartarone, P. Mustarelli, *Chem. Soc. Rev.* **2011**, *40*, 2525–2540.
[5] V. Thangadurai, D. Pinzaru, S. Narayanan, A. K. Baral, *J. Phys. Chem. Lett.* **2015**, *6*, 292–299.
[6] Z. Gao, H. Sun, L. Fu, F. Ye, Y. Zhang, W. Luo, Y. Huang, *Adv. Mater.* **2018**, *30*, e1705702.
[7] N. Kamaya, K. Homma, Y. Yamakawa, M. Hirayama, R. Kanno, M. Yonemura, T. Kamiyama, Y. Kato, S. Hama, K. Kawamoto, A. Mitsui, *Nat. Mater.* **2011**, *10*, 682–686.
[8] J. W. Fergus, *J. Power Sources* **2010**, *195*, 4554–4569.
[9] P. Oh, H. Lee, S. Park, H. Cha, J. Kim, J. Cho, *Adv. Energy Mater.* **2020**, *10*, 2000904.
[10] W. Zhang, F. H. Richter, S. P. Culver, T. Leichtweiss, J. G. Lozano, C. Dietrich, P. G. Bruce, W. G. Zeier, J. Janek, *ACS Appl. Mater. Interfaces* **2018**, *10*, 22226–22236.
[11] R. Koerver, I. Aygün, T. Leichtweiß, C. Dietrich, W. Zhang, J. O. Binder, P. Hartmann, W. G. Zeier, J. Janek, *Chem. Mater.* **2017**, *29*, 5574–5582.
[12] S. Lou, Q. Liu, F. Zhang, Q. Liu, Z. Yu, T. Mu, Y. Zhao, J. Borovilas, Y. Chen, M. Ge, X. Xiao, W. K. Lee, G. Yin, Y. Yang, X. Sun, J. Wang, *Nat. Commun.* **2020**, *11*, 5700.
[13] J. A. Lewis, F. J. Q. Cortes, Y. Liu, J. C. Miers, A. Verma, B. S. Vishnugopi, J. Tippens, D. Prakash, T. S. Marchese, S. Y. Han, C. Lee, P. P. Shetty, H. W. Lee, P. Shevchenko, F. De Carlo, C. Saldana, P. P. Mukherjee, M. T. McDowell, *Nat. Mater.* **2021**, *20*, 503–510.

[14] Y. Li, D. Zhang, X. Xu, Z. Wang, Z. Liu, J. Shen, J. Liu, M. Zhu, *J. Energy Chem.* **2021**, *60*, 32–60.
[15] Y. Wang, J. Roller, R. Maric, *Electrochim. Acta* **2017**, *241*, 510–516.
[16] J. Lin, L. Lin, S. Qu, D. Deng, Y. Wu, X. Yan, Q. Xie, L. Wang, D. Peng, *Energy Environ. Sci.* **2021**, *5*, 133–156.
[17] A. Patil, V. Patil, D. Wook Shin, J.-W. Choi, D.-S. Paik, S.-J. Yoon, *Mater. Res. Bull.* **2008**, *43*, 1913–1942.
[18] J. M. Zheng, X. B. Wu, Y. Yang, *Electrochim. Acta* **2011**, *56*, 3071–3078.
[19] S. Lobe, A. Bauer, S. Uhlenbruck, D. Fattakhova-Rohlfing, *Adv. Sci.* **2021**, *8*, e2002044.
[20] T. Hayashi, J. Okada, E. Toda, R. Kuzuo, Y. Matsuda, N. Kuwata, J. Kawamura, *J. Power Sources* **2015**, *285*, 559–567.
[21] X. Wang, G. Yushin, *Energy Environ. Sci.* **2015**, *8*, 1889–1904.
[22] X. Meng, X.-Q. Yang, X. Sun, *Adv. Mater.* **2012**, *24*, 3589–3615.
[23] Forge Nano. ALD-enabled battery materials for commercial applications integrating demonstrated and emerging value propositions. 2021. www.forgenano.com/wp-content/uploads/2021/01/ALD-For-Batteries.pdf.
[24] Y. Zhao, L. Zhang, J. Liu, K. Adair, F. Zhao, Y. Sun, T. Wu, X. Bi, K. Amine, J. Lu, X. Sun, *Chem. Soc. Rev.* **2021**, *50*, 3889–3956.
[25] Y. Zhao, X. Sun, *ACS Energy Lett.* **2018**, *3*, 899–914.
[26] Y. Zhao, K. Zheng, X. Sun, *Joule* **2018**, *2*, 2583–2604.
[27] S. M. George, *Chem. Rev.* **2010**, *110*, 111–131.
[28] J. Liu, X. Sun, *Nanotechnology* **2015**, *26*, 024001.
[29] L. Han, C.-T. Hsieh, B. Chandra Mallick, J. Li, Y. Ashraf Gandomi, *Nanoscale Adv.* **2021**, *3*, 2728–2740.
[30] Y. Kato, S. Hori, T. Saito, K. Suzuki, M. Hirayama, A. Mitsui, M. Yonemura, H. Iba, R. Kanno, *Nat. Energy* **2016**, *1*, 1–7.
[31] D. H. S. Tan, A. Banerjee, Z. Chen, Y. S. Meng, *Nat. Nanotechnol.* **2020**, *15*, 170–180.
[32] S.-K. Jung, H. Gwon, S.-S. Lee, H. Kim, J. C. Lee, J. G. Chung, S. Y. Park, Y. Aihara, D. Im, *J. Mater. Chem. A* **2019**, *7*, 22967–22976.
[33] Y. Zhu, X. He, Y. Mo, *ACS Appl. Mater. Interfaces* **2015**, *7*, 23685–23693.
[34] B. Zheng, X. Liu, J. Zhu, J. Zhao, G. Zhong, Y. Xiang, H. Wang, W. Zhao, E. Umeshbabu, Q.-H. Wu, J. Huang, Y. Yang, *Nano Energy* **2020**, *67*, 104252.
[35] F. Han, Y. Zhu, X. He, Y. Mo, C. Wang, *Adv. Energy Mater.* **2016**, *6*, 1501590.
[36] R. Koerver, W. Zhang, L. de Biasi, S. Schweidler, A. O. Kondrakov, S. Kolling, T. Brezesinski, P. Hartmann, W. G. Zeier, J. Janek, *Energy Environ. Sci.* **2018**, *11*, 2142–2158.
[37] X. Liu, B. Zheng, J. Zhao, W. Zhao, Z. Liang, Y. Su, C. Xie, K. Zhou, Y. Xiang, J. Zhu, H. Wang, G. Zhong, Z. Gong, J. Huang, Y. Yang, *Adv. Energy Mater.* **2021**, *11*, 2003583.
[38] H. Wang, J. Zhu, Y. Su, Z. Gong, Y. Yang, *Sci. China Chem.* **2021**, *64*, 879–898.
[39] J. Zhu, J. Zhao, Y. Xiang, M. Lin, H. Wang, B. Zheng, H. He, Q. Wu, J. Y. Huang, Y. Yang, *Chem. Mater.* **2020**, *32*, 4998–5008.
[40] H. Wang, H. Gao, X. Chen, J. Zhu, W. Li, Z. Gong, Y. Li, M. S. Wang, Y. Yang, *Adv. Energy Mater.* **2021**, *11*, 2102148.
[41] a) J. Y. Seok, A. S. Cavanagh, A. C. Dillon, M. D. Groner, S. M. George, *J. Korean Ceram. Soc.* **2010**, *47*, 61–65; b) Y. S. Jung, A. S. Cavanagh, L. A. Riley, S. H. Kang, A. C. Dillon, M. D. Groner, S. M. George, S. H. Lee, *Adv. Mater.* **2010**, *22*, 2172–2176.
[42] J. H. Woo, J. E. Trevey, A. S. Cavanagh, Y. S. Choi, S. C. Kim, S. M. George, K. H. Oh, S.-H. Lee, *J. Electrochem. Soc.* **2012**, *159*, A1120–A1124.
[43] S. P. Culver, R. Koerver, W. G. Zeier, J. Janek, *Adv. Energy Mater.* **2019**, *9*, 1900626.
[44] B. Wang, Y. Zhao, M. N. Banis, Q. Sun, K. R. Adair, R. Li, T. K. Sham, X. Sun, *ACS Appl. Mater. Interfaces* **2018**, *10*, 1654–1661.
[45] X. Meng, J. Liu, X. Li, M. N. Banis, J. Yang, R. Li, X. Sun, *RSC Adv.* **2013**, *3*, 7285.
[46] J. Liu, M. N. Banis, X. Li, A. Lushington, M. Cai, R. Li, T.-K. Sham, X. Sun, *J. Phys. Chem. C* **2013**, *117*, 20260–20267.
[47] B. Wang, J. Liu, M. Norouzi Banis, Q. Sun, Y. Zhao, R. Li, T. K. Sham, X. Sun, *ACS Appl. Mater. Interfaces* **2017**, *9*, 31786–31793.
[48] B. Wang, J. Liu, Q. Sun, R. Li, T. K. Sham, X. Sun, *Nanotechnology* **2014**, *25*, 504007.
[49] F. Zhao, Y. Zhao, J. Wang, Q. Sun, K. Adair, S. Zhang, J. Luo, J. Li, W. Li, Y. Sun, X. Li, J. Liang, C. Wang, R. Li, H. Huang, L. Zhang, S. Zhao, S. Lu, X. Sun, *Energy Storage Mater.* **2020**, *33*, 139–146.
[50] X. Li, Z. Ren, M. N. Banis, S. Deng, Y. Zhao, Q. Sun, C. Wang, X. Yang, W. Li, J. Liang, X. Li, Y. Sun, K. Adair, R. Li, Y. Hu, T.-K. Sham, H. Huang, L. Zhang, S. Lu, J. Luo, X. Sun, *ACS Energy Lett.* **2019**, *4*, 2480–2488.
[51] S. Deng, Y. Sun, X. Li, Z. Ren, J. Liang, K. Doyle-Davis, J. Liang, W. Li, M. Norouzi Banis, Q. Sun, R. Li, Y. Hu, H. Huang, L. Zhang, S. Lu, J. Luo, X. Sun, *ACS Energy Lett.* **2020**, *5*, 1243–1251.
[52] S. Deng, X. Li, Z. Ren, W. Li, J. Luo, J. Liang, J. Liang, M. N. Banis, M. Li, Y. Zhao, X. Li, C. Wang, Y. Sun, Q. Sun, R. Li, Y. Hu, H. Huang, L. Zhang, S. Lu, J. Luo, X. Sun, *Energy Storage Mater.* **2020**, *27*, 117–123.
[53] X. Liu, J. Shi, B. Zheng, Z. Chen, Y. Su, M. Zhang, C. Xie, M. Su, Y. Yang, *ACS Appl. Mater. Interfaces* **2021**, *13*, 41669–41679.
[54] D. Kitsche, Y. Tang, Y. Ma, D. Goonetilleke, J. Sann, F. Walther, M. Bianchini, J. Janek, T. Brezesinski, *ACS Appl. Energ. Mater.* **2021**, *4*, 7338–7345.
[55] Y. Liu, Q. Sun, J. Liu, M. Norouzi Banis, Y. Zhao, B. Wang, K. Adair, Y. Hu, Q. Xiao, C. Zhang, L. Zhang, S. Lu, H. Huang, X. Song, X. Sun, *ACS Appl. Mater. Interfaces* **2020**, *12*, 2293–2298.
[56] K. Takada, N. Ohta, L. Zhang, K. Fukuda, I. Sakaguchi, R. Ma, M. Osada, T. Sasaki, *Solid State Ionics* **2008**, *179*, 1333–1337.
[57] X. Li, L. Jin, D. Song, H. Zhang, X. Shi, Z. Wang, L. Zhang, L. Zhu, *J. Energy Chem.* **2020**, *40*, 39–45.
[58] E. Kazyak, K.-H. Chen, K. N. Wood, A. L. Davis, T. Thompson, A. R. Bielinski, A. J. Sanchez, X. Wang, C. Wang, J. Sakamoto, N. P. Dasgupta, *Chem. Mater.* **2017**, *29*, 3785–3792.
[59] X. Han, Y. Gong, K. K. Fu, X. He, G. T. Hitz, J. Dai, A. Pearse, B. Liu, H. Wang, G. Rubloff, Y. Mo, V. Thangadurai, E. D. Wachsman, L. Hu, *Nat. Mater.* **2017**, *16*, 572–579.
[60] Y. Liu, Q. Sun, Y. Zhao, B. Wang, P. Kaghazchi, K. R. Adair, R. Li, C. Zhang, J. Liu, L. Y. Kuo, Y. Hu, T. K. Sham, L. Zhang, R. Yang, S. Lu, X. Song, X. Sun, *ACS Appl. Mater. Interfaces* **2018**, *10*, 31240–31248.
[61] C. Wang, Y. Zhao, Q. Sun, X. Li, Y. Liu, J. Liang, X. Li, X. Lin, R. Li, K. R. Adair, L. Zhang, R. Yang, S. Lu, X. Sun, *Nano Energy* **2018**, *53*, 168–174.
[62] S. Rajendran, A. Pilli, O. Omolere, J. Kelber, L. M. R. Arava, *Chem. Mater.* **2021**, *33*, 3401–3412.
[63] C. Wang, Y. Gong, B. Liu, K. Fu, Y. Yao, E. Hitz, Y. Li, J. Dai, S. Xu, W. Luo, E. D. Wachsman, L. Hu, *Nano Lett.* **2017**, *17*, 565–571.
[64] S. J. Lee, H. K. Balk, S. M. Lee, *Electrochem. Commun.* **2003**, *5*, 32–35.
[65] G. Yang, C. Abraham, Y. Ma, M. Lee, E. Helfrick, D. Oh, D. Lee, *Appl. Sci.-Basel.* **2020**, *10*, 4247.
[66] M. Armand, J. M. Tarascon, *Nature* **2008**, *451*, 652–657.
[67] Z. Takehara, Z. Ogumi, Y. Uchimoto, E. Endo, Y. Kanamori, *J. Electrochem. Soc.* **1991**, *138*, 1574–1582.
[68] H. Ohtsuka, Y. Sakurai, *Solid State Ionics.* **2001**, *144*, 59–64.
[69] M. Baba, N. Kumagai, H. Kobayashi, O. Nakano, K. Nishidate, *Electrochem. Solid-State Lett.* **1999**, *2*, 320–322.
[70] M. E. Donders, W. M. Arnoldbik, H. C. M. Knoops, W. M. M. Kessels, P. H. L. Notten, *J. Electrochem. Soc.* **2013**, *160*, A3066–A3071.
[71] V. Miikkulainen, A. Ruud, E. Østreng, O. Nilsen, M. Laitinen, T. Sajavaara, H. Fjellvåg, *J. Phys. Chem. C* **2013**, *118*, 1258–1268.
[72] J. Liu, M. N. Banis, Q. Sun, A. Lushington, R. Li, T. K. Sham, X. Sun, *Adv. Mater.* **2014**, *26*, 6472–6477.
[73] M. Nisula, M. Karppinen, *J. Mater. Chem. A* **2018**, *6*, 7027–7033.
[74] R. Sheil, D. Butts, K. Jungjohann, J. Yoo, B. Dunn, J. P. Chang, *J. Vac. Sci. Technol. A* **2021**, *39*, 012408.
[75] M. Nisula, M. Karppinen, *Nano Lett.* **2016**, *16*, 1276–1281.
[76] J. Heiska, M. Nisula, E. L. Rautama, A. J. Karttunen, M. Karppinen, *Dalton Trans.* **2020**, *49*, 1591–1599.
[77] J. Multia, J. Heiska, A. Khayyami, M. Karppinen, *ACS Appl. Mater. Interfaces* **2020**, *12*, 41557–41566.
[78] J. Liu, J. Wang, *Front. Energy Res.* **2021**, *9*, 665884.
[79] J. Song, Q. H. Wu, Q. F. Dong, M. S. Zheng, S. T. Wu, S. G. Sun, *Prog. Chem.* **2007**, *19*, 66–73.
[80] A. C. Kozen, A. J. Pearse, C.-F. Lin, M. Noked, G. W. Rubloff, *Chem. Mater.* **2015**, *27*, 5324–5331.
[81] M. Nisula, Y. Shindo, H. Koga, M. Karppinen, *Chem. Mater.* **2015**, *27*, 6987–6993.
[82] A. J. Pearse, T. E. Schmitt, E. J. Fuller, F. El-Gabaly, C.-F. Lin, K. Gerasopoulos, A. C. Kozen, A. A. Talin, G. Rubloff, K. E. Gregorczyk, *Chem. Mater.* **2017**, *29*, 3740–3753.
[83] A. Pearse, T. Schmitt, E. Sahadeo, D. M. Stewart, A. Kozen, K. Gerasopoulos, A. A. Talin, S. B. Lee, G. W. Rubloff, K. E. Gregorczyk, *ACS Nano* **2018**, *12*, 4286–4294.
[84] Y.-C. Perng, J. Cho, S. Y. Sun, D. Membreno, N. Cirigliano, B. Dunn, J. P. Chang, *J. Mater. Chem. A* **2014**, *2*, 9566–9573.
[85] T. Aaltonen, M. Alnes, O. Nilsen, L. Costelle, H. Fjellvåg, *J. Mater. Chem.* **2010**, *20*.
[86] Y. Cao, X. Meng, J. W. Elam, *ChemElectroChem* **2016**, *3*, 858–863.

[87] E. Kazyak, K.-H. Chen, A. L. Davis, S. Yu, A. J. Sanchez, J. Lasso, A. R. Bielinski, T. Thompson, J. Sakamoto, D. J. Siegel, N. P. Dasgupta, *J. Mater. Chem. A* **2018**, *6*, 19425–19437.
[88] H. Wang, K. E. Gregorczyk, S. B. Lee, G. W. Rubloff, C.-F. Lin, *J. Phys. Chem. C* **2020**, *124*, 6830–6837.
[89] E. Kazyak, M. Shin, W. S. LePage, T. H. Cho, N. P. Dasgupta, *Chem. Commun.* **2020**, *56*, 15537–15540.
[90] S. H. Jung, K. Oh, Y. J. Nam, D. Y. Oh, P. Bruener, K. Kang, Y. S. Jung, *Chem. Mater.* **2018**, *30*, 8190–8200.
[91] B. Fleutot, B. Pecquenard, H. Martinez, M. Letellier, A. Levasseur, *Solid State Ionics* **2011**, *186*, 29–36.

Manuscript received: August 13, 2022
Revised manuscript received: November 3, 2022
Accepted manuscript online: November 10, 2022
Version of record online: December 5, 2022